

Thin Films of Conjugated Chalcogenadiazole: Growth, Structure, and Optical Properties of Substituted Selenadiazoloquinoline

Anton Pylypenko,[⊥] Elena Chulanova,^{*,⊥} Frederik Unger, Jakob Keck, Ivan Zaluzhnyy, Ingrid Dax, Matthias Schwartzkopf, Alexander Gerlach,^{*} Alexander Hinderhofer, Alfred J. Meixner, and Frank Schreiber^{*}



Cite This: *J. Phys. Chem. C* 2024, 128, 8104–8113



Read Online

ACCESS |



Metrics & More

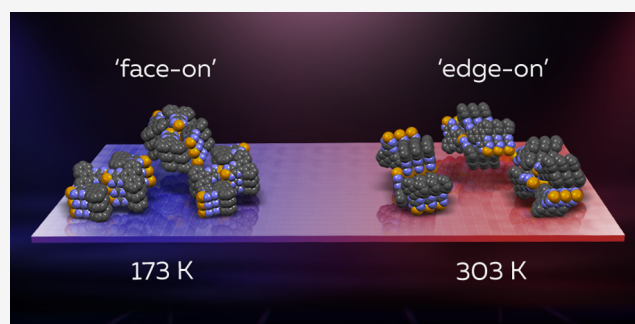


Article Recommendations



Supporting Information

ABSTRACT: Thin films of π -conjugated organic molecules are of high interest for organic optoelectronics. Due to their strong and tunable absorption spectrum and good charge carrier mobilities, thiadiazolo-heteroacenes are considered to be a prospective class of materials for these applications. Additional chemical modification of these molecules by heavy Se atoms and extending the π -conjugation hold promise to further tune the optical properties and structural arrangement through the heavy atom effect and secondary interactions. Therefore, understanding the thin film growth behavior as well as the optical properties of such derivatives is crucial for future applications. In this study, thin films of dibenzoselenadiazoloquinoline (dbSeQ) were grown under ultra-high vacuum conditions by organic molecular beam deposition on native silicon oxide substrates at different temperatures. Their optical properties, structure, and morphology were examined by optical spectroscopy, time-resolved fluorescence spectroscopy, ellipsometry, time-resolved surface-sensitive X-ray scattering, and microscopy techniques.



INTRODUCTION

In the past years, there has been significant interest in organic semiconductors based on polymers and π -conjugated small molecules, due to their great potential for applications in electronics and optoelectronics.^{1–5} A key feature of these materials is their tunability through chemical modification, *i.e.*, the opportunity to change the properties by adding or substituting specific functional groups. Particularly, differently substituted 1,2,5-thia- and selenadiazoles are widely used as an electron-accepting core in materials for field-effect transistors,^{6–8} solar cells,^{9,10} and light-emitting diodes¹¹ due to their electron-deficient heteroaromatic moieties with rigid planarity. The unique molecular structure of 1,2,5-selenadiazoles enables these molecules to aggregate into supramolecular synthons forming characteristic Se \cdots N square motifs through chalcogen bonding,¹² which has received, among other secondary bonding interactions, growing attention in the last two decades.^{13,14} This bonding originates from the interaction of the σ -holes (regions of positive electrostatic potential) centered on selenium atoms with the lone pairs of nitrogen atoms acting as a Lewis base.¹⁵ The strength and directionality of this bonding allow the formation of dimers and polymers, with the possibility of electron transfer between molecules and the formation of well-ordered structures.^{13,14,16–18} This aspect is important, as the molecular ordering within the material critically determines charge transport, energy transfer, and

optical properties and, consequently, defines and controls the overall performance of the device.^{19–21} To additionally strengthen this feature, the self-association of π -conjugated molecules through effective π – π stacking interactions can be employed to achieve morphological organization and structural order at mesoscopic length scales.²² In this regard, a rational design strategy to achieve perfect crystallinity within the material involves extending the conjugated framework by incorporating aromatic systems into the chalcogenadiazole moiety. This approach not only enables the modulation of the electronic structure but also strengthens self-association properties, arising from the enlarged π -surface.

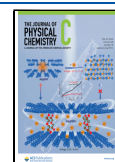
Previously studied π -conjugated polymers that incorporate a chalcogenadiazole scaffold typically exhibit disordered thin films.^{23,24} As a result, an increased focus on exploring small-molecule derivatives has emerged^{7,25–27} as they offer not only better crystallinity, but also several additional benefits, including low polydispersity, well-defined chemical structures, and reliable synthetic reproducibility.¹

Received: March 7, 2024

Revised: April 18, 2024

Accepted: April 22, 2024

Published: May 2, 2024



A further aspect concerning the arrangement of molecules within the material pertains to the dependency of the electrical and optical characteristics of thin films (and, therefore, device efficiency) on the molecular orientation relative to the substrate, which has been observed in particular for π -conjugated molecules of low symmetry.^{28–32} Thus, a comprehensive understanding and effective control over molecular orientation are highly desirable to unlock the full potential of these materials in prospective applications.

Here, we present a structural and optical characterization of π -extended dibenzo[*f,h*][1,2,5]selenadiazolo[3,4-*b*]-quinoxaline³³ (dbSeQ, Figure 1, left) in thin films prepared

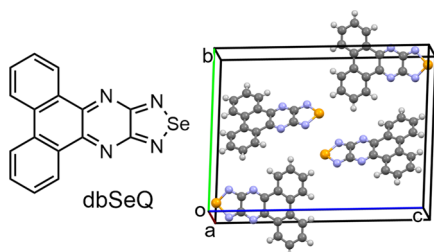


Figure 1. Chemical structure of dbSeQ (left) and its unit cell (right, unpublished results).

by organic molecular beam deposition (OMBD).^{34–36} We investigated the molecular ordering and orientation relative to the silica substrate at different temperatures exploiting *ex* and *in situ* grazing-incidence small- and wide-angle X-ray scattering (GISAXS and GIWAXS, respectively) combined with atomic force microscopy (AFM). Our findings confirm that by substrate temperature control during the growth of thin

films, we can achieve a distinct alteration in the molecular orientation of the dbSeQ molecules within the films, directly impacting their morphology and optical properties.

MATERIALS AND METHODS

The dbSeQ was synthesized and provided by the group of Prof. Zibarev (Novosibirsk Institute of Organic Chemistry) and used as received. Thin films of dbSeQ were grown using OMBD^{34–36} under ultra-high vacuum conditions (base pressure = 1×10^{-8} mbar) in a portable vacuum chamber.³⁷ Two different types of substrates were used: commercial silicon wafers with a native oxide layer (Si(100), p-type) for X-ray and AFM characterization and fused silica wafers for the ultraviolet–visible (UV–vis) absorption and photoluminescence (PL) measurements. The substrates were cleaned in an ultrasonic bath with acetone and isopropanol for 10 min each, followed by heating up to 480 K inside the vacuum chamber for 12 h. The substrate temperature during the growth was maintained at 303 K (room temperature, RT) or 173 K (low temperature, LT). The growth rates of the thin films were monitored using an SQM-160 quartz crystal microbalance (Inficon, Bad Ragaz, Switzerland) and calibrated by X-ray reflectivity (GE XRD3003 diffractometer, using Cu $K\alpha_1$ radiation) and spectroscopic ellipsometry (M-2000 V, J.A. Woolam). The surface morphology of the thin films was characterized by AFM NanoWizard II (JPK Instruments, Berlin, Germany) in tapping mode. The scans were performed at several positions of the sample surface and the scanning area of a single scan was $10 \times 10 \mu\text{m}^2$. The AFM data were analyzed using the Gwyddion software package.³⁸

In situ GIWAXS and GISAXS measurements were conducted at the beamline P03 at DESY (Hamburg,

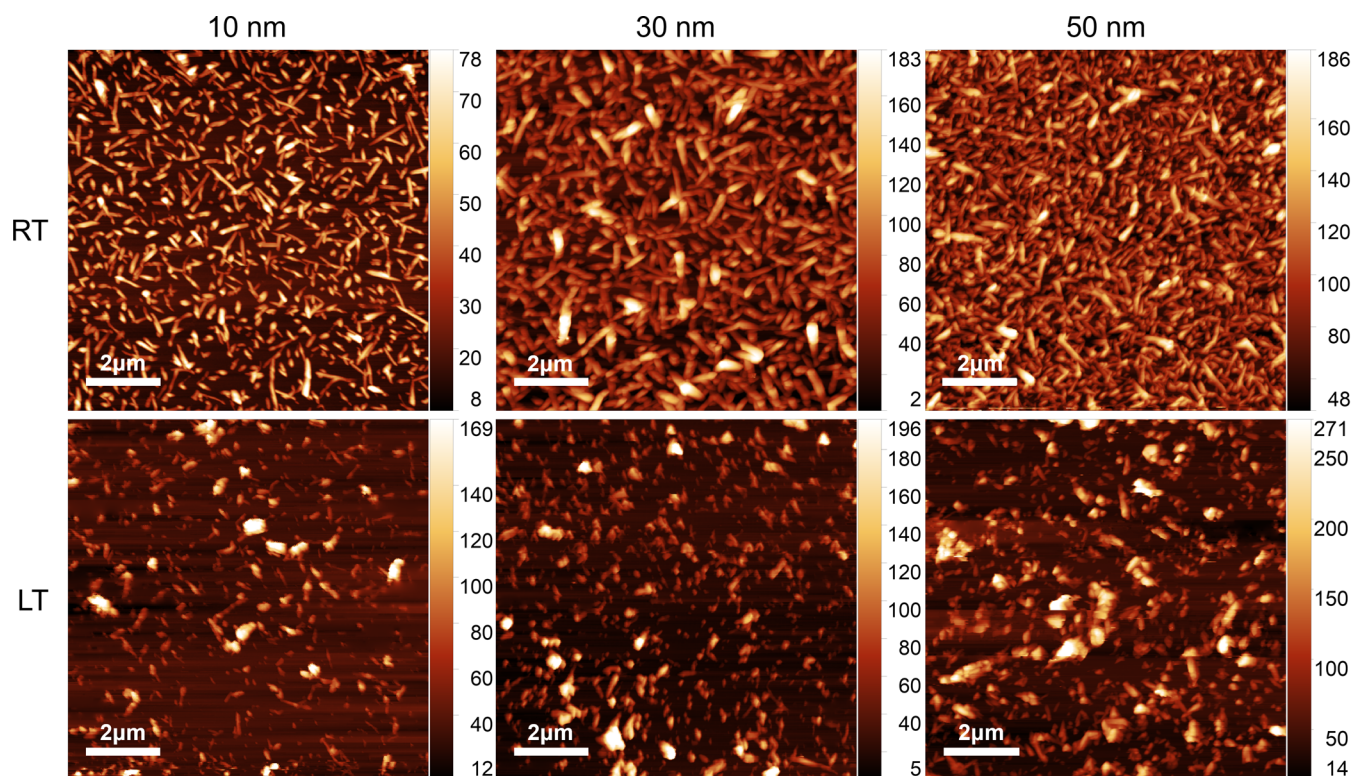


Figure 2. AFM images of dbSeQ thin films grown at RT (top) and LT (bottom) with different thicknesses. The 50 nm films were grown at a high deposition rate of 1 nm/min. The growth rate of all other samples was 0.3 nm/min. The height scale is in nm.

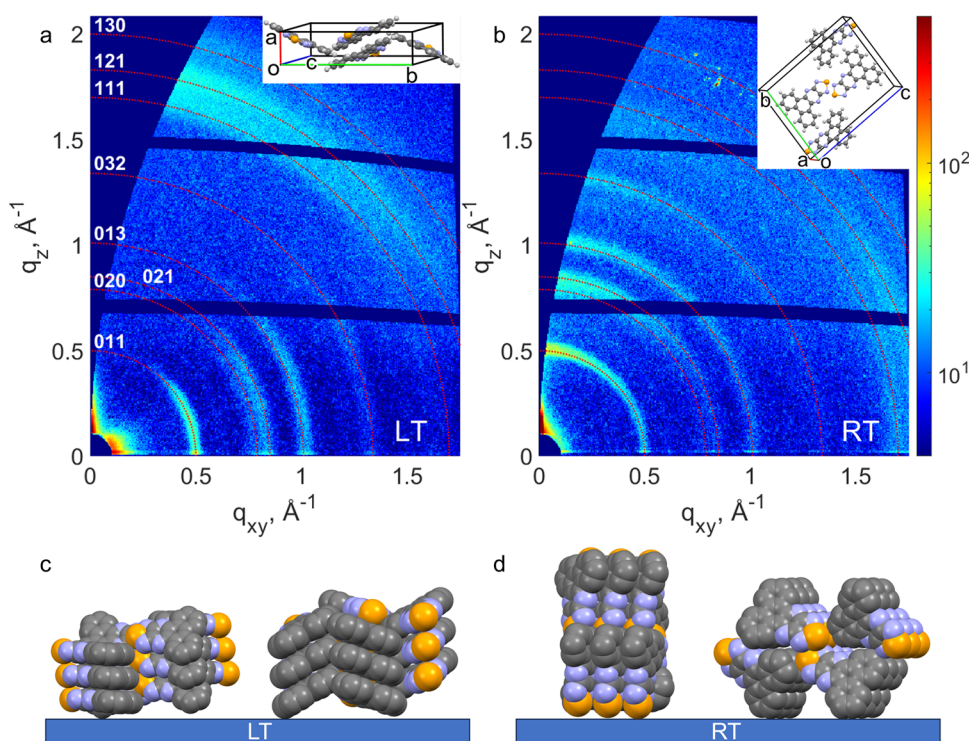


Figure 3. Reciprocal space maps of dbSeQ thin films with 50 nm thicknesses grown at LT (a) and RT (b). The red dotted rings mark the position of the diffraction peaks of dbSeQ based on the single-crystal structure (unpublished results). Sketches of the structure of dbSeQ thin films on native Si oxide: (c) grown at LT, with preferred face-on orientation; (d) grown at RT, with preferred edge-on orientation, both exhibiting some angular distribution of crystallites. The insets illustrate the predominant orientations of the dbSeQ unit cell, namely, (011) plane parallel to the substrate at LT, and perpendicular to the substrate at RT.

Germany)³⁹ by using a focused beam ($27 \times 25 \mu\text{m}^2$) with a wavelength of 1.044 \AA at an incidence angle of 0.4° . A LAMBDA 9 M (X-Spectrum, Hamburg, Germany) detector at a sample-to-detector distance of $\sim 205 \text{ mm}$ was used for the GIWAXS measurements and a PILATUS 2M (Dectris, Baden-Daettwil, Switzerland) detector at a sample-to-detector distance of $\sim 4115 \text{ mm}$ was used for the GISAXS measurements. Furthermore, samples were characterized *ex situ* by GIWAXS and GISAXS using a Xeuss 2.0 (Xenocs, Grenoble, France) laboratory instrument with $\lambda = 1.541 \text{ \AA}$ at an incidence angle of 0.2° with a PILATUS 300 K two-dimensional (2D) detector (Dectris, Baden-Daettwil, Switzerland). The data were processed using DPDAK⁴⁰ and GIXSGUI software.⁴¹

The steady-state UV–vis absorption spectra were obtained using a PerkinElmer Lambda 950 UV–vis–NIR spectrometer in transmission mode. Photoluminescence spectra were recorded with a Labram HR 800 spectrometer (Horiba Jobin Yvon, France) with a CCD $1024 \times 256 \text{ pixel}^2$ detector and a frequency-doubled Nd:YAG excitation laser with a wavelength of 532 nm . Temperature-dependent PL spectra were obtained with a cooling CryoVac system with liquid nitrogen in the range from 80 to 290 K. Fluorescence lifetime measurements were performed at 77 K in an optical cryostat (SVT-200, Janis) with a custom-built confocal microscope⁴² equipped with an air objective lens ($\text{NA} = 0.85$, Newport), a spectrometer (Shamrock, Andor Technology, U.K.) with a thermoelectrically cooled (203 K) CCD camera, and a single photon avalanche diode (SPAD, PDM series, Micro Photon Devices, Italy). Samples were excited by a 485 nm pulsed laser diode (PicoQuant GmbH, Germany) with a pulse width of $<100 \text{ ps}$ at a repetition rate of 40 MHz with linear polarization. The

excitation light was blocked by a 488 nm long-pass filter. For two-channel measurements, a 635 nm dichroic beam splitter was inserted into the detection path, directing the emission light onto two separate MPD photodiodes. Time-correlated single photon counting (TCSPC) histograms were recorded using the HydraHarp 400 system (PicoQuant GmbH, Germany). The instrument response was measured in reflection at the laser emission line with neutral density filters for laser attenuation. The SymPhoTime64 software package was used to evaluate the TCSPC data which were collected from nine repeated measurements at different positions of the sample for the RT thin film and from 10 repeated measurements for the LT thin film.

The UV–vis spectrum of dbSeQ was calculated using optimized geometries at the time-dependent density functional theory (TD-DFT) level of theory⁴³ with the double-hybrid B2PLYP method⁴⁴ and the def2-tzvp basis set^{45,46} using the Becke–Johnson damping function for dispersion correction.^{47,48} The RIJCOSX approximation was used to speed up computations.^{49,50} All calculations were performed with the ORCA program package (version 4.2.0).^{51,52}

RESULTS AND DISCUSSION

Surface Morphologies. The morphologies of the *ex situ* films with a nominal dbSeQ thickness of 10, 30, and 50 nm grown at 303 K (RT) and at 173 K (LT) were investigated by AFM. Figure 2 shows representative AFM topography images of the thin films.

For thin films grown at RT with a 10 nm nominal thickness, small needle-like structures are observed, which grow in size upon the deposition of the material, reaching the length of 2

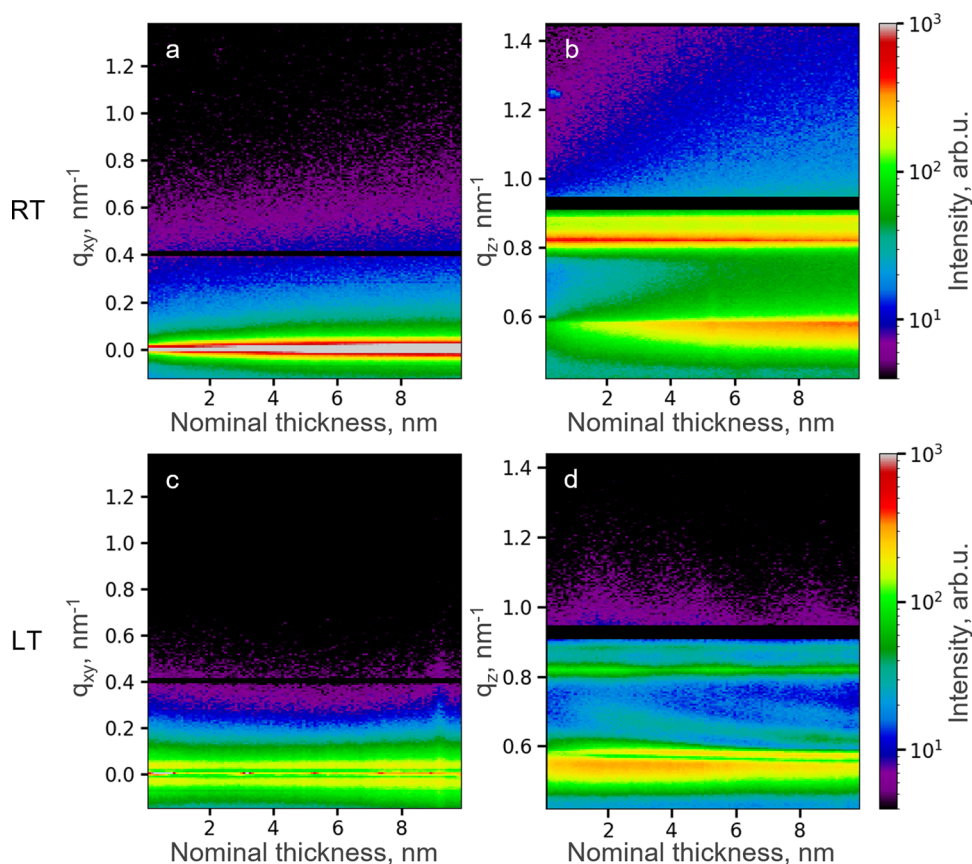


Figure 4. Contour plots of horizontal (a, c) and vertical (b, d) line cuts of 2D GISAXS data versus the nominal thickness of dbSeQ thin film deposited at RT and LT, respectively.

μm for a thin film with a nominal thickness of 30 nm. This indicates a preferred one-dimensional (1D) packing which most probably is formed by π -stacks of dbSeQ randomly oriented along the surface of the substrate. The molecular orientation will be discussed in detail in the [Structure of the Thin Films](#) Section. For a thin film with a nominal thickness of 50 nm grown at a high deposition rate of 1 nm/min, smaller needles are observed, which cover the whole substrate. The same behavior was observed for thinner dbSeQ films grown at an identical deposition rate. A qualitatively similar decrease in the grain size and an increase in the surface smoothness with an increase in deposition rate was also observed earlier both for organic materials⁵³ and metals.⁵⁴

In the case of LT growth, a distinct change in the morphology of the dbSeQ thin film is evident, resulting in the formation of sparsely distributed islands on the surface. This change can be attributed to a different orientation of the molecules during deposition at lower substrate temperatures, a phenomenon previously observed in other extended organic semiconductors.^{30,55} As the film thickness increases, these islands tend to grow vertically, while their area does not increase significantly. Thus, they cover only about 50% of the substrate surface, even in films with a nominal thickness of 50 nm. Based on the AFM pictures, it can be inferred that the dbSeQ molecules prefer to interact with neighboring molecules rather than the silicon substrate's native oxide layer, as the latter interaction is energetically less favorable.

Due to the rugged nature of films grown at LT, performing a quantitative grain analysis is not feasible. For a quantitative analysis of the growth of dbSeQ at RT, the AFM images were

analyzed based on height–height correlation functions (HHCFs).^{56,57} HHCFs of each sample were fitted with $f(x) = 2\sigma^2[1 - \exp(-(x/\xi)^{2\alpha})]$, where σ is the root-mean-squared (RMS) roughness, α is the Hurst parameter, and ξ is the lateral correlation length. The values from the fitting of the HHCF were averaged over several AFM images. An example of the data evaluation with this method is provided in the SI ([Figure S1](#)).

The Hurst parameter equals 0.82 ± 0.1 , indicating fast roughening in the films.^{56,57} The RMS roughness rises together with increasing nominal film thickness, $\sigma_{10\text{nm}} = 13.8 \text{ nm}$, $\sigma_{30\text{nm}} = 31.0 \text{ nm}$. The lateral correlation length follows the same tendency: $\xi_{10\text{nm}} = 98.1 \text{ nm}$, $\xi_{30\text{nm}} = 157.8 \text{ nm}$, which quantifies the visually observed increase in grain sizes. We note that for the 50 nm thick film grown at a high rate (1 nm/min) both, RMS roughness and lateral correlation coefficient are relatively low ($\sigma_{50\text{nm}} = 22.6 \text{ nm}$, $\xi_{50\text{nm}} = 118.3 \text{ nm}$), which agrees with the aforementioned smaller grain size and higher smoothness of the film.

Thus, for dbSeQ, there is an obvious dependence of the thin film morphology on the substrate temperature during growth. At RT, nanorods reaching a size of up to 2 μm and growing along the substrate surface are obtained, while at LT, growth of high, separated islands of the material is observed.

Structure of the Thin Films. To investigate the molecular structure of dbSeQ thin films, we used GIWAXS and GISAXS techniques. The reciprocal space maps obtained from GIWAXS measurements of the thin films with a nominal thickness of 50 nm grown at RT and LT are shown in [Figure 3](#). We note that the pattern observed for films with nominal

thicknesses of 10 and 30 nm remains essentially the same, only the intensity increases proportionally with the thickness. The observed diffraction peaks and rings correspond to the previously obtained single-crystal structure of dbSeQ (unpublished results). A notable difference between the films grown at LT and RT lies in the orientation of $(0kl)$ diffraction peaks, which are centered around $q_z = 0 \text{ \AA}^{-1}$ for LT films and around $q_{xy} = 0 \text{ \AA}^{-1}$ for RT films. The angular distribution of the diffracted intensity of Bragg peaks belonging to the (011) plane exhibits a full width at half-maximum (fwhm) of 51° for the LT film and 41° for the RT films (SI, Figure S2), which indicates not very strong but noticeable alignment. Concurrently, the signal originating from the $(1kl)$ planes exhibits a contrasting behavior, with the majority of diffracted intensity aligned along $q_{xy} = 0 \text{ \AA}^{-1}$ for the LT film and along $q_z = 0 \text{ \AA}^{-1}$ for the RT film.

Therefore, the dbSeQ crystalline domains grown at LT are predominantly oriented in such a way that the b and c unit cell axes are parallel to the substrate surface. The a axis is then perpendicular to the substrate plane, and the molecules inside a unit cell exhibit a tilted face-on configuration (Figure 3c). In the case of RT growth, the unit cell is tilted by 90° so that the (011) plane is oriented perpendicular to the substrate surface, while the a axis is parallel to the substrate surface. In this orientation, the molecules are standing with a tilted edge-on configuration (Figure 3d). This yields π -stacks of the molecules growing along the substrate surface at RT, and perpendicular at LT, in agreement with the AFM data.

Overall, the structural differences of the dbSeQ films grown at LT and RT closely resemble those previously reported for pentacene, diindenoperylene, and α -sexithiophene,^{30,55} albeit with a higher degree of mosaicity. For these results, it was suggested³⁰ that due to the lack of thermal energy at lower substrate temperatures, molecules initially adopting a face-on orientation to maximize van der Waals interactions with the substrate are unable to perform a transition to an edge-on orientation that occurs at RT.^{58,59} However, this implies energetically favorable interaction with the surface and formation of closed monolayers, which is opposed to the AFM data for the dbSeQ films grown at LT. Therefore, one can assume the presence of more complicated equilibria between substrate-molecule and π -stacking interactions leading to the formation of separated high islands.

For a more comprehensive understanding of the variations in the morphologies and growth kinetics of the thin films of dbSeQ grown at different temperatures, we conducted *in situ* GISAXS during the OMBD of dbSeQ on a silicon substrate. This technique allows probing the nanoscale structure over macroscopic areas.⁶⁰

To analyze the vertical growth of the islands, slightly off-centered vertical (out-of-plane) line cuts of 2D GISAXS data were made at $q_{xy} = 0.03 \text{ nm}^{-1}$ (position is indicated by the red dashed line in Figure S3a). Similarly, to investigate changes in horizontal arrangement, horizontal (in-plane) line cuts were made at the Yoneda peak region (corresponding to the critical angle of the material) at $q_z = 0.578 \text{ nm}^{-1}$ (as indicated by the black dashed line in Figure S3a). Figure 4a,b presents 2D plots of these in- and out-of-plane cuts versus the nominal thickness of the RT deposited film. There are neither prominent side peaks in horizontal line cuts nor additional peaks in the vertical line cuts for the RT-grown film, indicating a rough surface and the absence of a characteristic island size distribution. The broadening of the Yoneda peak in q_{xy} is observed during the

deposition, which is related to diffuse scattering from the rough surface and indicates the broader distribution of the domain sizes for increasing nominal film thickness.⁶¹ Selected 2D GISAXS patterns obtained during the deposition of dbSeQ thin film at RT and respective line cuts are represented in the SI (Figure S3a–c).

The GISAXS patterns look notably different for the dbSeQ deposition at LT of the substrate (Figure S3d). At the beginning of the deposition, two symmetrical broad side peaks appear at low q_{xy} (Figures 4c, and S3e) and remain there until the end of deposition, which indicates the presence of relatively widely distributed in-plane characteristic length scales for the features on the surface.⁶² The island-to-island distance D was estimated by fitting the side peak position and using the relation $D \approx 2\pi q_{xy}^{-1}$.⁶² According to the fitting results, there is a very small monotonic shift of the side peak position toward higher q_{xy} values during the deposition (Figure S4b) and its broadening, giving values of D decreasing from 156 ± 5 nm at the beginning to 149 ± 6 nm at the end of the deposition. Additionally, the vertical line cuts (Figures 4d and S3f) also show prominent peaks along q_z shifting toward lower q_z during the deposition. All this indicates a single growth regime for the LT growth with small changes in the island-to-island distance distribution and predominant growth of the islands in the vertical direction.

To see if there are temperature-induced changes in the morphology of the LT-grown film with a nominal film thickness of 30 nm upon heating up to RT, we took several GISAXS images: after the end of the growth at LT, 10 min after reaching RT and 60 min after reaching RT (Figure 5). The analysis of the horizontal line cuts (Figure 5b) made in the same manner as for *in situ* measurements shows that there is an increase in island-to-island distance from 149 ± 6 nm after the growth at LT to 202 ± 2 nm after thermalizing for 60 min at RT, what is probably caused by the coalescence of adjacent domains. Fringes in intensity along q_z (Figure 5c) are explained by the X-ray waveguide effect resulting from conformal roughness between the substrate and the dbSeQ thin film layer.^{63,64}

Optical Properties. Figure 6 displays the UV–vis absorption spectra measured for dbSeQ thin films with a nominal thickness of 30 nm deposited on glass substrates at LT and RT. Similar to previously published results for analogous π -extended chalcogenadiazoles,^{26,65,66} the absorption spectrum for the dbSeQ thin film grown at RT is notably broadened and red-shifted when compared to the dbSeQ absorption spectrum in solution (unpublished results), but in general resembles the shape of the spectrum. Specifically, a pronounced peak is observed at 2.85 eV (peak B), accompanied by two peaks of lower intensity at 2.5 eV (peak A) and 3.17 eV (peak C). Additionally, sub-optical band gap absorbance can be related to light scattering from the rough surface of the organic thin films.

For the LT film, the positions of the peaks remain practically unchanged (Figure 6). The most notable differences occur in the relative intensity of the peaks. Peak C becomes the most prominent for the LT film, while the relative intensity of peaks A and B decreases. Additionally, a minor blue shift is observed for peak B. Considering the GIWAXS data, we attribute peaks B and C to different electronic transitions with differently oriented transition dipole moments. Therefore, the tilt of the molecules toward the substrate and a considerable degree of mosaicity can make changes in optical spectra for RT and LT

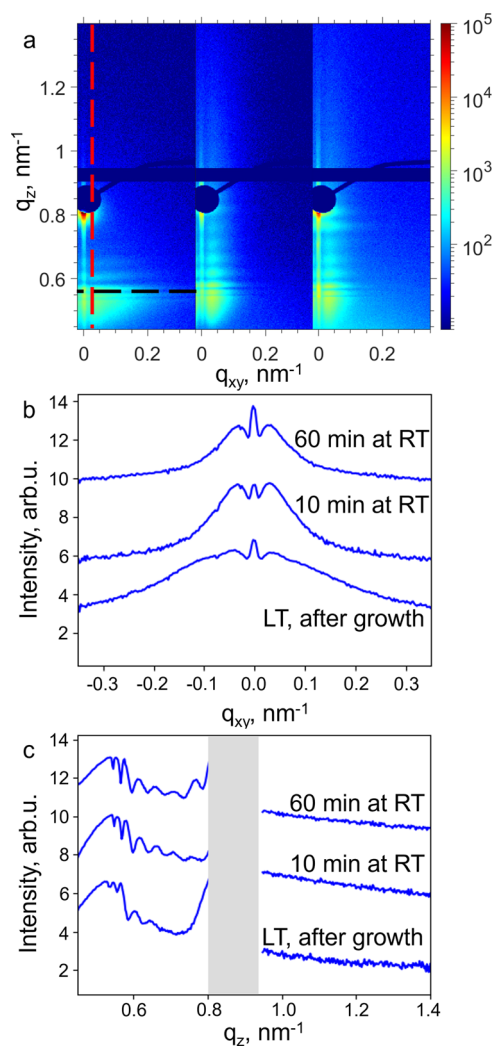


Figure 5. 2D GISAXS patterns of the dbSeQ thin film after the growth at LT (a, left), thermalized at RT for 10 min (a, center) and 60 min (a, right) together with their horizontal (b) and vertical (c) line cuts. Black and red dashed lines in (a) represent the horizontal and vertical line cut directions, respectively. The gray rectangle in (c) corresponds to the beam stop and intermodular gap of the detector.

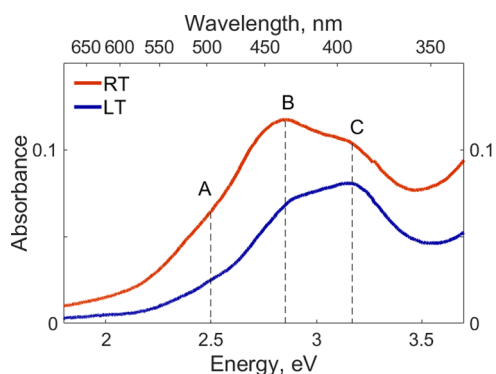


Figure 6. UV-vis absorption spectra of dbSeQ thin films with a nominal thickness of 30 nm grown at RT and LT.

thin films of dbSeQ less pronounced. The interpretation of the optical spectra of dbSeQ is intricate, and routine DFT calculations performed for a single molecule in the gas phase (Figure S5) do not satisfactorily reproduce the experimental

spectra, whereas more sophisticated calculations are beyond the scope of the paper.

For a more in-depth characterization of the optical properties of dbSeQ, we conducted temperature-dependent PL measurements. Since we employed a 532 nm laser for excitation, only the low-energy shoulder of the long-wavelength peak A gets excited. At 290 K, the PL spectra of dbSeQ grown at both RT and LT (Figure 7a) exhibit three discernible bands: D (1.75 eV), E (1.87 eV), and F (2.07 eV). The preeminent emission peak for the RT film is peak F, with peaks D and E contributing to a broad tail toward lower energies. Worth mentioning is the relatively substantial Stokes shift of 0.43 eV, a phenomenon previously observed in selenium-containing chalcogenadiazoles.⁶⁷

In the case of the LT film, we again observe changes in the relative intensities of the emission bands: the intensity of band F decreases, while bands D and E become more prominent. These distinctions between the spectra of films grown at RT and LT become even more pronounced in the spectra obtained at 80 K (Figure 7b). Alongside the peak narrowing, a distinct change in their relative intensities is observed. Specifically, the intensity of band F notably diminishes in the LT-grown film, while the intensity of band D increases. Similarly, for the RT-grown film, we observe a comparable tendency in these changes, albeit with band F maintaining a comparatively high intensity.

Time-correlated single photon counting (TCSPC) was employed to analyze the time-resolved fluorescence kinetics of thin films of dbSeQ. The acquired data (see Figure S6) were fitted with a biexponential decay curve (with reduced chi-squared values less than 1.2), revealing short (<600 ps)- and long (>1.5 ns)-lifetime contributions. Given the susceptibility of short-lifetime contributions to artifacts arising from varying pulse travel times due to dispersion in the optical elements of the microscope and short-lifetime components originating from the microscope's instrument response (see Figure S7), only the long-lifetime contribution was utilized in the analysis.

To discern the differences between peaks D, E, and F, we compared data collected across the entire emission spectrum (Figure 8) with data obtained using a dichroic beam splitter at 635 nm (1.95 eV, Figure 8). This configuration allowed us to isolate the signal of peak F and the small tail of peak E, directed to the short-pass (SP) channel, from the optical signature of peaks D and E, which are directed to the long-pass (LP) channel (Figure S8). Notably, the higher relative intensity of peak F in the RT thin film is accompanied by a longer median lifetime of luminescence directed to the SP channel (2.49 ns for RT, 2.42 ns for LT), suggesting that band F has a longer lifetime than band E. Simultaneously, in the spectral region belonging to the LP channel, the relative intensity of band D was higher for the LT thin film, accompanied by a longer median lifetime of luminescence (2.22 ns for LT, 2.05 ns for RT). This observation leads us to conclude that the lifetime of peak D is longer than that of peak E. Additionally, the overall luminescence lifetime is higher for the LT thin films (2.32 ns for LT, 2.13 ns for RT), aligning with our assumptions, as the LP channel contributes more significantly to the total lifetime than the SP channel (Figure S8). Taken together, these findings suggest that all three peaks are of different electronic nature.

However, the exact electronic nature of the involved excited state remains elusive. Overall, the thin films of dbSeQ constitute a material with intricate optical properties,

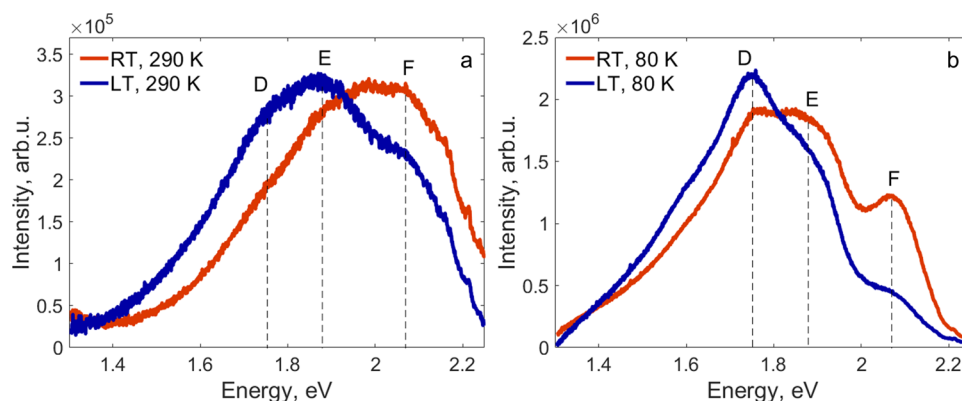


Figure 7. PL spectra of dbSeQ thin films with a nominal thickness of 30 nm grown at RT and LT obtained at 290 K (a) and 80 K (b).

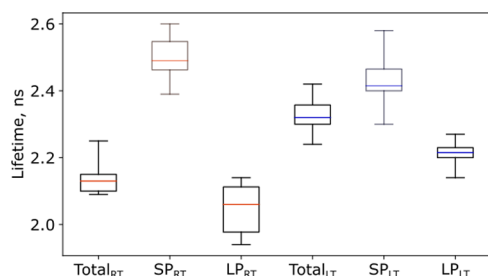


Figure 8. Luminescence lifetimes of dbSeQ thin films with a nominal thickness of 30 nm grown at RT and LT, measured over the entire emission spectral range (Total) and with a beam splitter at 635 nm separating the signal to short-pass (SP < 635 nm) and long-pass (LP > 635 nm) channels. Data were collected at 77 K upon excitation at 485 nm. The boxplots represent the long-lifetime contribution obtained by fitting the time-resolved luminescence with a biexponential decay function. The whiskers indicate the lowest and highest lifetime values.

demanding a further thorough investigation and posing a challenge for theoretical understanding.

CONCLUSIONS AND SUMMARY

We conducted a comprehensive investigation of the growth, molecular structure, and optical properties of vacuum-deposited dbSeQ at both cryogenic and ambient substrate temperatures. Our findings reveal that dbSeQ tends to form a thin film of low crystallinity, which is evident from the presence of Debye–Scherrer rings rather than single diffraction peaks. However, our experimental results indicate that the preferred orientation of the crystallites on the substrate can be substantially altered by changing the substrate temperature. At room temperature, thin films exhibit a predominant edge-on orientation of the molecules toward the substrate, resulting in the three-dimensional (3D) growth of islands and the formation of needle-like structures. Conversely, at low temperatures, there is a transition of molecular orientation toward a predominant face-on configuration, leading to a distinct grain morphology and higher surface roughness. *In situ* GISAXS data confirmed different growth regimes at room and low temperatures and showed that at low temperatures, grains are distant from each other and adopt the substrate morphology. This change in orientation also induces changes in the optical spectra of the thin films.

We demonstrate control over the molecular orientation on the substrate and consequently properties of the material *via*

changes in the substrate temperature. The introduction of this new material holds great promise for optoelectronic devices, underscoring the broad applicability of the template-free approach in achieving diverse molecular orientations for thin films with well-defined crystalline properties.

ASSOCIATED CONTENT

Supporting Information

The Supporting Information is available free of charge at <https://pubs.acs.org/doi/10.1021/acs.jpcc.4c01515>.

Additional details about AFM; GIWAXS, GISAXS, and TCSPC measurements; calculated electronic transitions (PDF)

AUTHOR INFORMATION

Corresponding Authors

Elena Chulanova – Institut für Angewandte Physik, Universität Tübingen, 72076 Tübingen, Germany; orcid.org/0000-0001-5452-6831; Email: chulanovaea@gmail.com

Alexander Gerlach – Institut für Angewandte Physik, Universität Tübingen, 72076 Tübingen, Germany; Center for Light-Matter Interaction, Sensors and Analytics LISA+, Universität Tübingen, 72076 Tübingen, Germany; orcid.org/0000-0003-1787-1868; Email: alexander.gerlach@uni-tuebingen.de

Frank Schreiber – Institut für Angewandte Physik, Universität Tübingen, 72076 Tübingen, Germany; Center for Light-Matter Interaction, Sensors and Analytics LISA+, Universität Tübingen, 72076 Tübingen, Germany; orcid.org/0000-0003-3659-6718; Email: frank.schreiber@uni-tuebingen.de

Authors

Anton Pylypenko – Institut für Angewandte Physik, Universität Tübingen, 72076 Tübingen, Germany

Frederik Unger – Institut für Angewandte Physik, Universität Tübingen, 72076 Tübingen, Germany; orcid.org/0000-0002-7127-3829

Jakob Keck – Institut für Physikalische und Theoretische Chemie, Universität Tübingen, 72076 Tübingen, Germany

Ivan Zaluzhnyy – Institut für Angewandte Physik, Universität Tübingen, 72076 Tübingen, Germany; orcid.org/0000-0001-5946-2777

Ingrid Dax – Institut für Angewandte Physik, Universität Tübingen, 72076 Tübingen, Germany

Matthias Schwartzkopf – Deutsches Elektronen-Synchrotron DESY, 22607 Hamburg, Germany; orcid.org/0000-0002-2115-9286

Alexander Hinderhofer – Institut für Angewandte Physik, Universität Tübingen, 72076 Tübingen, Germany; orcid.org/0000-0001-8152-6386

Alfred J. Meixner – Institut für Physikalische und Theoretische Chemie, Universität Tübingen, 72076 Tübingen, Germany; orcid.org/0000-0002-0187-2906

Complete contact information is available at:
<https://pubs.acs.org/10.1021/acs.jpcc.4c01515>

Author Contributions

[†]A.P. and E.C. contributed equally to this work.

Notes

The authors declare no competing financial interest.

ACKNOWLEDGMENTS

The authors acknowledge financial support by the German Research Foundation (DFG). Part of this research was conducted at the P03 beamline of PETRA III at DESY, a member of the Helmholtz Association (HGF).

REFERENCES

- Mishra, A.; Bäuerle, P. Small Molecule Organic Semiconductors on the Move: Promises for Future Solar Energy Technology. *Angew. Chem., Int. Ed.* **2012**, *51* (9), 2020–2067.
- Wang, C.; Dong, H.; Hu, W.; Liu, Y.; Zhu, D. Semiconducting π -Conjugated Systems in Field-Effect Transistors: A Material Odyssey of Organic Electronics. *Chem. Rev.* **2012**, *112* (4), 2208–2267.
- Wadsworth, A.; Moser, M.; Marks, A.; Little, M. S.; Gasparini, N.; Brabec, C. J.; Baran, D.; McCulloch, I. Critical Review of the Molecular Design Progress in Non-Fullerene Electron Acceptors towards Commercially Viable Organic Solar Cells. *Chem. Soc. Rev.* **2019**, *48* (6), 1596–1625.
- He, Y.; Li, N.; Brabec, C. J. Single-Component Organic Solar Cells with Competitive Performance. *Org. Mater.* **2021**, *03* (02), 228–244.
- Zhang, G.; Lin, F. R.; Qi, F.; Heumüller, T.; Distler, A.; Egelhaaf, H.-J.; Li, N.; Chow, P. C. Y.; Brabec, C. J.; Jen, A. K. Y.; Yip, H. L. Renewed Prospects for Organic Photovoltaics. *Chem. Rev.* **2022**, *122* (18), 14180–14274.
- Xia, D.; Wang, X.-Y.; Guo, X.; Baumgarten, M.; Li, M.; Müllen, K. Fused Bis-Benzothiadiazoles as Electron Acceptors. *Cryst. Growth Des.* **2016**, *16* (12), 7124–7129.
- Cortizo-Lacalle, D.; Gozálvez, C.; Olano, M.; Sun, X.; Melle-Franco, M.; Hueso, L. E.; Mateo-Alonso, A. Bisthiadiazole-Fused Tetraazapentacenequinone: An Air-Stable Solution-Processable n-Type Organic Semiconductor. *Org. Lett.* **2015**, *17* (23), 5902–5905.
- Gu, P.-Y.; Zhang, J.; Long, G.; Wang, Z.; Zhang, Q. Solution-Processable Thiadiazoloquinoline-Based Donor–Acceptor Small Molecules for Thin-Film Transistors. *J. Mater. Chem. C* **2016**, *4* (17), 3809–3814.
- Jung, J. W.; Jo, J. W.; Jung, E. H.; Jo, W. H. Recent Progress in High Efficiency Polymer Solar Cells by Rational Design and Energy Level Tuning of Low Bandgap Copolymers with Various Electron-Withdrawing Units. *Org. Electron.* **2016**, *31*, 149–170.
- Mori, H. Development of Semiconducting Polymers Based on a Novel Heteropolycyclic Aromatic Framework. *Polym. J.* **2021**, *53* (9), 975–987.
- Neto, B. A. D.; Lapis, A. A. M.; da Silva Júnior, E. N.; Dupont, J. 2,1,3-Benzothiadiazole and Derivatives: Synthesis, Properties, Reactions, and Applications in Light Technology of Small Molecules. *Eur. J. Org. Chem.* **2013**, *2013* (2), 228–255.
- Wang, W.; Ji, B.; Zhang, Y. Chalcogen Bond: A Sister Noncovalent Bond to Halogen Bond. *J. Phys. Chem. A* **2009**, *113* (28), 8132–8135.
- Alfuth, J.; Zadykiewicz, B.; Sikorski, A.; Połoński, T.; Eichstaedt, K.; Olszewska, T. Effect of Aromatic System Expansion on Crystal Structures of 1,2,5-Thia- and 1,2,5-Selenadiazoles and Their Quaternary Salts: Synthesis, Structure, and Spectroscopic Properties. *Materials* **2020**, *13* (21), No. 4908, DOI: [10.3390/ma13214908](https://doi.org/10.3390/ma13214908).
- Cozzolino, A. F.; Vargas-Baca, I.; Mansour, S.; Mahmoudkhani, A. H. The Nature of the Supramolecular Association of 1,2,5-Chalcogenadiazoles. *J. Am. Chem. Soc.* **2005**, *127* (9), 3184–3190.
- Murray, J. S.; Lane, P.; Clark, T.; Politzer, P. σ -hole bonding: molecules containing group VI atoms. *J. Mol. Model.* **2007**, *13* (10), 1033–1038.
- Bui, A. H.; Pulle, A. D. F.; Micallef, A. S.; Lessard, J. J.; Tuten, B. T. Dynamic Chalcogen Squares for Material and Topological Control over Macromolecules. *Angew. Chem., Int. Ed.* **2024**, No. e202404474, DOI: [10.1002/anie.202404474](https://doi.org/10.1002/anie.202404474).
- Radiush, E. A.; Wang, H.; Chulanova, E. A.; Ponomareva, Y. A.; Li, B.; Wei, Q. Y.; Salmikov, G. E.; Petrakova, S. Y.; Semenov, N. A.; Zibarev, A. V. Halide Complexes of 5,6-Dicyano-2,1,3-Benzoselenadiazole with 1:4 Stoichiometry: Cooperativity between Chalcogen and Hydrogen Bonding. *ChemPlusChem* **2023**, *88* (11), No. e202300523.
- Eichstaedt, K.; Wasilewska, A.; Wicher, B.; Gdaniec, M.; Połoński, T. Supramolecular Synthesis Based on a Combination of Se...N Secondary Bonding Interactions with Hydrogen and Halogen Bonds. *Cryst. Growth Des.* **2016**, *16* (3), 1282–1293.
- Li, H.; Giri, G.; Tok, J. B. H.; Bao, Z. Toward High-Mobility Organic Field-Effect Transistors: Control of Molecular Packing and Large-Area Fabrication of Single-Crystal-Based Devices. *MRS Bull.* **2013**, *38* (1), 34–42.
- Kim, D.; Lee, S.; Park, J.; Lee, J.; Choi, H. C.; Kim, K.; Ryu, S. In-Plane and Out-of-Plane Excitonic Coupling in 2D Molecular Crystals. *Nat. Commun.* **2023**, *14* (1), No. 2736.
- Hagara, J.; Kim, H.; Hagenlocher, J.; Zaluzhnyy, I.; Gerlach, A.; Hinderhofer, A.; Roth, S. V.; Brütting, W.; Schreiber, F. Improved Order and Transport in C60 Thin Films Grown on SiO2 via Use of Transient Templates. *Appl. Phys. Lett.* **2022**, *121* (18), No. 182101.
- Chen, Z.; Lohr, A.; Saha-Möller, C. R.; Würthner, F. Self-Assembled π -Stacks of Functional Dyes in Solution: Structural and Thermodynamic Features. *Chem. Soc. Rev.* **2009**, *38* (2), 564–584.
- Dallos, T.; Beckmann, D.; Bruncklaus, G.; Baumgarten, M. Thiadiazoloquinoline–Acetylene Containing Polymers as Semiconductors in Ambipolar Field Effect Transistors. *J. Am. Chem. Soc.* **2011**, *133* (35), 13898–13901.
- Steckler, T. T.; Henriksson, P.; Mollinger, S.; Lundin, A.; Salleo, A.; Andersson, M. R. Very Low Band Gap Thiadiazoloquinoline Donor–Acceptor Polymers as Multi-tool Conjugated Polymers. *J. Am. Chem. Soc.* **2014**, *136* (4), 1190–1193.
- An, C.; Zhou, S.; Baumgarten, M. Condensed Derivatives of Thiadiazoloquinoline as Strong Acceptors. *Cryst. Growth Des.* **2015**, *15* (4), 1934–1938.
- Kato, S.-i.; Watanabe, K.; Tamura, M.; Ueno, M.; Nitani, M.; Ie, Y.; Aso, Y.; Yamanobe, T.; Uehara, H.; Nakamura, Y. Tetraalkoxyphenanthrene-Fused Thiadiazoloquinolines: Synthesis, Electronic, Optical, and Electrochemical Properties, and Self-Assembly. *J. Org. Chem.* **2017**, *82* (6), 3132–3143.
- Müller, M.; Koser, S.; Tverskoy, O.; Rominger, F.; Freudenberg, J.; Bunz, U. H. F. Thiadiazolo-Azaacenes. *Chem. - Eur. J.* **2019**, *25* (24), 6082–6086.
- Sirringhaus, H.; Brown, P. J.; Friend, R. H.; Nielsen, M. M.; Bechgaard, K.; Langeveld-Voss, B. M. W.; Spiering, A. J. H.; Janssen, R. A. J.; Meijer, E. W.; Herwig, P.; de Leeuw, D. M. Two-Dimensional Charge Transport in Self-Organized, High-Mobility Conjugated Polymers. *Nature* **1999**, *401* (6754), 685–688.
- Amsterdam, S. H.; LaMountain, T.; Stanev, T. K.; Sangwan, V. K.; López-Arteaga, R.; Padgaonkar, S.; Watanabe, K.; Taniguchi, T.; Weiss, E. A.; Marks, T. J.; et al. Tailoring the Optical Response of

- Pentacene Thin Films via Templated Growth on Hexagonal Boron Nitride. *J. Phys. Chem. Lett.* **2021**, *12* (1), 26–31.
- (30) Duva, G.; Mann, A.; Pithan, L.; Beyer, P.; Hagenlocher, J.; Gerlach, A.; Hinderhofer, A.; Schreiber, F. Template-Free Orientation Selection of Rod-Like Molecular Semiconductors in Polycrystalline Films. *J. Phys. Chem. Lett.* **2019**, *10* (5), 1031–1036.
- (31) Hofmann, A.; Schmid, M.; Brütting, W. The Many Facets of Molecular Orientation in Organic Optoelectronics. *Adv. Opt. Mater.* **2021**, *9* (21), No. 2101004.
- (32) Heinemeyer, U.; Broch, K.; Hinderhofer, A.; Kytka, M.; Scholz, R.; Gerlach, A.; Schreiber, F. Real-Time Changes in the Optical Spectrum of Organic Semiconducting Films and Their Thickness Regimes during Growth. *Phys. Rev. Lett.* **2010**, *104* (25), No. 257401.
- (33) Konstantinova, L. S.; Bobkova, I. E.; Nelyubina, Y. V.; Chulanova, E. A.; Irtegov, I. G.; Vasilieva, N. V.; Camacho, P. S.; Ashbrook, S. E.; Hua, G.; Slawin, A. M. Z.; et al. [1,2,5]Selenadiazolo[3,4-b]pyrazines: Synthesis from 3,4-Diamino-1,2,5-selenadiazole and Generation of Persistent Radical Anions. *Eur. J. Org. Chem.* **2015**, *2015* (25), 5585–5593.
- (34) Forrest, S. R. Ultrathin Organic Films Grown by Organic Molecular Beam Deposition and Related Techniques. *Chem. Rev.* **1997**, *97* (6), 1793–1896.
- (35) Schreiber, F. Organic Molecular Beam Deposition: Growth Studies Beyond the First Monolayer. *Phys. Status Solidi A* **2004**, *201* (6), 1037–1054.
- (36) Kowarik, S.; Gerlach, A.; Schreiber, F. Organic Molecular Beam Deposition: Fundamentals, Growth Dynamics, and In Situ Studies. *J. Phys.: Condens. Matter* **2008**, *20* (18), No. 184005.
- (37) Ritley, K. A.; Krause, B.; Schreiber, F.; Dosch, H. A Portable Ultrahigh Vacuum Organic Molecular Beam Deposition System for In Situ x-Ray Diffraction Measurements. *Rev. Sci. Instrum.* **2001**, *72* (2), 1453–1457.
- (38) Nečas, D.; Klapetek, P. Gwyddion: an Open-Source Software for SPM Data Analysis. *Open Phys.* **2012**, *10* (1), 181–188.
- (39) Buffet, A.; Rothkirch, A.; Dohrmann, R.; Korstgens, V.; Kashem, M. M. A.; Perlich, J.; Herzog, G.; Schwartzkopf, M.; Gehrke, R.; Müller-Buschbaum, P.; Roth, S. V. P03, the Microfocus and Nanofocus X-Ray Scattering (MiNaXS) Beamline of the PETRA III Storage Ring: the Microfocus Endstation. *J. Synchrotron Radiat.* **2012**, *19* (4), 647–653, DOI: 10.1107/S0909049512016895.
- (40) Benecke, G.; Wagermaier, W.; Li, C.; Schwartzkopf, M.; Flucke, G.; Hoerth, R.; Zizak, I.; Burghammer, M.; Metwalli, E.; Müller-Buschbaum, P.; et al. A Customizable Software for Fast Reduction and Analysis of Large X-ray Scattering Data Sets: Applications of the New DPDAK Package to Small-Angle X-ray Scattering and Grazing-Incidence Small-Angle X-ray Scattering. *J. Appl. Crystallogr.* **2014**, *47* (5), 1797–1803.
- (41) Jiang, Z. GIXSGUI: a MATLAB Toolbox for Grazing-Incidence X-Ray Scattering Data Visualization and Reduction, and Indexing of Buried Three-Dimensional Periodic Nanostructured Films. *J. Appl. Crystallogr.* **2015**, *48* (3), 917–926.
- (42) Nosrati, S.; Wackenhut, F.; Kertzsch, C.; Brecht, M.; Meixner, A. J. Controlling Three-Color Förster Resonance Energy Transfer in an Optical Fabry–Pérot Microcavity at Low Mode Order. *J. Phys. Chem. C* **2023**, *127* (25), 12152–12159.
- (43) Dreuw, A.; Head-Gordon, M. Single-Reference ab Initio Methods for the Calculation of Excited States of Large Molecules. *Chem. Rev.* **2005**, *105* (11), 4009–4037.
- (44) Grimme, S.; Neese, F. Double-Hybrid Density Functional Theory for Excited Electronic States of Molecules. *J. Chem. Phys.* **2007**, *127* (15), No. 154116.
- (45) Weigend, F.; Ahlrichs, R. Balanced Basis Sets of Split Valence, Triple Zeta Valence and Quadruple Zeta Valence Quality for H to Rn: Design and Assessment of Accuracy. *Phys. Chem. Chem. Phys.* **2005**, *7* (18), 3297–3305.
- (46) Weigend, F. Accurate Coulomb-Fitting Basis Sets for H to Rn. *Phys. Chem. Chem. Phys.* **2006**, *8* (9), 1057–1065.
- (47) Grimme, S.; Antony, J.; Ehrlich, S.; Krieg, H. A Consistent and Accurate Ab Initio Parametrization of Density Functional Dispersion Correction (DFT-D) for the 94 Elements H–Pu. *J. Chem. Phys.* **2010**, *132* (15), No. 154104.
- (48) Grimme, S.; Ehrlich, S.; Goerigk, L. Effect of the Damping Function in Dispersion Corrected Density Functional Theory. *J. Comput. Chem.* **2011**, *32* (7), 1456–1465.
- (49) Hellweg, A.; Hättig, C.; Höfener, S.; Klopper, W. Optimized Accurate Auxiliary Basis Sets for RI-MP2 and RI-CC2 Calculations for the Atoms Rb to Rn. *Theor. Chem. Acc.* **2007**, *117* (4), 587–597.
- (50) Neese, F.; Wennmohs, F.; Hansen, A.; Becker, U. Efficient, Approximate and Parallel Hartree–Fock and Hybrid DFT Calculations. A ‘Chain-of-Spheres’ Algorithm for the Hartree–Fock Exchange. *Chem. Phys.* **2009**, *356* (1), 98–109.
- (51) Neese, F. The ORCA Program System. *WIREs Comput. Mol. Sci.* **2012**, *2* (1), 73–78.
- (52) Neese, F.; Wennmohs, F.; Becker, U.; Riplinger, C. The ORCA Quantum Chemistry Program Package. *J. Chem. Phys.* **2020**, *152* (22), No. 224108.
- (53) Storzer, T.; Hinderhofer, A.; Zeiser, C.; Novák, J.; Fišer, Z.; Belova, V.; Reisz, B.; Maiti, S.; Duva, G.; Hallani, R. K.; et al. Growth, Structure, and Anisotropic Optical Properties of Difluoro-anthradithiophene Thin Films. *J. Phys. Chem. C* **2017**, *121* (38), 21011–21017.
- (54) Schwartzkopf, M.; Hinz, A.; Polonskyi, O.; Strunskus, T.; Löhner, F. C.; Körstgens, V.; Müller-Buschbaum, P.; Faupel, F.; Roth, S. V. Role of Sputter Deposition Rate in Tailoring Nanogranular Gold Structures on Polymer Surfaces. *ACS Appl. Mater. Interfaces* **2017**, *9* (6), 5629–5637.
- (55) Shioya, N.; Murdey, R.; Nakao, K.; Yoshida, H.; Koganezawa, T.; Eda, K.; Shimoaka, T.; Hasegawa, T. Alternative Face-on Thin Film Structure of Pentacene. *Sci. Rep.* **2019**, *9* (1), No. 579.
- (56) Krug, J. Origins of Scale Invariance in Growth Processes. *Adv. Phys.* **1997**, *46* (2), 139–282.
- (57) Dürr, A. C.; Schreiber, F.; Ritley, K. A.; Kruppa, V.; Krug, J.; Dosch, H.; Struth, B. Rapid Roughening in Thin Film Growth of an Organic Semiconductor (Diindenoperylene). *Phys. Rev. Lett.* **2003**, *90* (1), No. 016104.
- (58) Zeng, Y.; Tao, B.; Yin, Z. Molecular Orientation Transformation of Pentacene on Amorphous SiO₂: A Computational Study on the Initial Growth Stage of Physical Vapor Deposition. *J. Cryst. Growth* **2014**, *405*, 73–80.
- (59) Zeng, Y.; Tao, B.; Chen, J.; Yin, Z. Temperature-Dependent Orientation Study of the Initial Growth of Pentacene on Amorphous SiO₂ by Molecular Dynamics Simulations. *J. Cryst. Growth* **2015**, *429*, 35–42.
- (60) Müller-Buschbaum, P. The Active Layer Morphology of Organic Solar Cells Probed with Grazing Incidence Scattering Techniques. *Adv. Mater.* **2014**, *26* (46), 7692–7709.
- (61) Schwartzkopf, M.; Santoro, G.; Brett, C. J.; Rothkirch, A.; Polonskyi, O.; Hinz, A.; Metwalli, E.; Yao, Y.; Strunskus, T.; Faupel, F.; et al. Real-Time Monitoring of Morphology and Optical Properties during Sputter Deposition for Tailoring Metal–Polymer Interfaces. *ACS Appl. Mater. Interfaces* **2015**, *7* (24), 13547–13556.
- (62) Schwartzkopf, M.; Buffet, A.; Körstgens, V.; Metwalli, E.; Schlage, K.; Benecke, G.; Perlich, J.; Rawolle, M.; Rothkirch, A.; Heidmann, B.; et al. From Atoms to Layers: In Situ Gold Cluster Growth Kinetics During Sputter Deposition. *Nanoscale* **2013**, *5* (11), 5053–5062.
- (63) Müller-Buschbaum, P.; Stamm, M. Correlated Roughness, Long-Range Correlations, and Dewetting of Thin Polymer Films. *Macromolecules* **1998**, *31* (11), 3686–3692.
- (64) Schwartzkopf, M.; Wöhner, S.-J.; Waclawek, V.; Carstens, N.; Rothkirch, A.; Rubeck, J.; Gensch, M.; Drewes, J.; Polonskyi, O.; Strunskus, T.; et al. Real-Time Insight into Nanostructure Evolution during the Rapid Formation of Ultra-Thin Gold Layers on Polymers. *Nanoscale Horiz.* **2021**, *6* (2), 132–138.
- (65) Alagna, N.; Han, J.; Wollscheid, N.; Lustres, J. L. P.; Herz, J.; Hahn, S.; Koser, S.; Paulus, F.; Bunz, U. H. F.; Dreuw, A.; et al. Tailoring Ultrafast Singlet Fission by the Chemical Modification of

Phenazinothiadiazoles. *J. Am. Chem. Soc.* **2019**, *141* (22), 8834–8845, DOI: 10.1021/jacs.9b01079.

(66) Lindner, B. D.; Coombs, B. A.; Schaffroth, M.; Engelhart, J. U.; Tverskoy, O.; Rominger, F.; Hamburger, M.; Bunz, U. H. F. From Thia- to Selenadiazoles: Changing Interaction Priority. *Org. Lett.* **2013**, *15* (3), 666–669.

(67) Coombs, B. A.; Lindner, B. D.; Edkins, R. M.; Rominger, F.; Beeby, A.; Bunz, U. H. F. Photophysical Property Trends for a Homologous Series of Bis-Ethynyl-Substituted Benzochalcogendiazoles. *New J. Chem.* **2012**, *36* (3), 550–553.